Series-parallel Sequence Impedance Models of Multi-loop Grid-forming Converters

Xiaokuan Jin, Jianhua Wang, Han Yan, Xijun Ni, Zhendong Ji, Baojian Ji, and Ding Wan

***Abstract*—The gradual penetration of grid-forming (GFM) converters into new power systems with renewable energy sources may result in the emergence of small-signal instability issues. These issues can be elucidated using sequence impedance models, which offer a more tangible and meaningful interpretation than *dq*-domain impedance models and state-space models. However, existing research has primarily focused on the impact of power loops and inner control loops in GFM converters, which has not yet elucidated the precise physical interpretation of inner voltage and current loops of GFM converters in circuits. This paper derives series-parallel sequence impedance models of multi-loop GFM converters, demonstrating that the voltage loop can be regarded as a parallel impedance and the current loop as a series impedance. Consequently, the corresponding small-signal stability characteristics can be identified through Bode diagrams of sequence impedances or by examining the physical meanings of impedances in series and in parallel. The results indicate that the GFM converter with a single power loop is a candidate suitable for application in new power systems, given its reduced number of control parameters and enhanced low-frequency performance, particularly in weak grids. The results of PLECS simulations and corresponding prototype experiments verify the accuracy of the analytical analysis under diverse grid conditions.**

***Index Terms*—Grid-forming (GFM) converter, sequence impedance, renewable energy source, small-signal stability.**

I. Introduction

THE increasing penetration of renewable energy sources into power grids and the high demand for switching between grid-connected and off-grid states have led to a widespread use of power electronic converters. However, this widespread use may result in harmonic oscillation and other interaction stability problems [1], [2]. Power electronic converters can be classified into grid-forming (GFM) and grid-following (GFL) converters. The GFM converters exhibit superior dynamic responses and weak grid adaptability due to their synchronous-generator-like characteristics [3], [4].

In practical application, it should be noted that GFM converters are produced by different companies and therefore have relatively different multiple control loops. The power outer-loops of GFM converters, which include droop control, power synchronization control (PSC), virtual synchronous generator (VSG) control, and matching control (MC), exhibit similar impedance behaviors [5]. Conversely, the inner-loops exhibit a wider bandwidth and are typically ten times faster than the power outer-loops, which are previously simplified or even discarded. Nevertheless, these inner-loops do affect the oscillation frequency and damping of converters [6].

The stability mechanism of multi-loop GFM converters, including small-signal stability under diverse grid conditions, can be analyzed by state-space modeling or impedance modeling [7]. The state-space models of GFM converters consider a great number of state variables and the state-space matrices have a high dimension. Although the dominant eigenvalues can be modified through the introduction of control parameters, the physical meanings of the models remain opaque, presenting challenges for subsequent improvements [8]. The impedance modeling can reduce the dimension of state-space matrices, and an impedance model of GFM converters considering the power loop and the voltage and current dual-loop on the AC side has been established in the *dq*-frame [9]. The impedance circuit model in the *dq*-frame is also proposed to separate multiple control loops into virtual circuit elements [10]. However, the intricate effects of virtual circuit elements on converter stability persist. The multitude of circuit elements in series and in parallel gives rise to a higher dimensionality of models, which in turn creates a challenge to directly display the characteristics of voltage and current controllers. Moreover, the impedances in the *dq*-frame possess more vague physical meanings than sequence impedances [11], which can be more accurately measured through the injection of harmonics, whether simulated or experimental. Although the impedances of converters in the *dq*-frame can be transformed into positive- and negative-sequence impedances through linear matrix transformation [12], the sequence impedances can reflect more nonlinear information including harmonic stability.

The sequence impedance model, particularly the positive-sequence impedance model, tends to be a method more suit-

Manuscript received: June 25, 2024; revised: October 15, 2024; accepted: December 5, 2024. Date of CrossCheck: December 5, 2024. Date of online publication: January 29, 2025.

This work was supported by the National Defense Basic Scientific Research Program of China (No. JCKY2021606B014).

X. Jin, J. Wang (corresponding author), and H. Yan are with School of Electrical Engineering, Southeast University, Nanjing 210096, China (e-mail: jinxiaokuan@seu.edu.cn; wangjianhua@seu.edu.cn; yanhan124@seu.edu.cn).

X. Ni and D. Wan are with School of Electric Power Engineering, Nanjing Institute of Technology, Nanjing 211167, China (e-mail: nxj@njit. edu. cn; y00450230829@njit.edu.cn).

Z. Ji and B. Ji are with School of Automation, Nanjing University of Science and Technology, Nanjing 210094, China (e-mail: zhendong_ji@njust.edu.cn; jibaojian@njust.edu.cn).

DOI: 10.35833/MPCE.2024.000676

able for analyzing the small-signal stability of GFM converters. This model divides the grid-connected converter system into two impedances: one representing the grid and the other representing the converter [13]. This simplified system model is valid for the purpose of collectively determining possible resonances between the grid and the converter. Furthermore, the model necessitates the nonlinearity in at least part of the system, as illustrated by the impedance alteration in response to varying control parameters such as inertia and damping and system parameters such as grid impedance. However, the observed behavior is distinctively different from similar oscillatory responses that have been previously investigated in the domain of nonlinear system theory [13]. Consequently, the sequence impedances can reflect nonlinear information in small-signal stability analysis, particularly when considering the distinct linear or nonlinear resistive or inductive characteristics in the GFM converter connected to the grid.

Previous sequence impedance models [14]-[17] have considered the characteristics of different power loops and control parameters of GFM converters. Reference [14] proposes a sequence impedance model of the GFM converter with voltage and current control loops. Reference [15] employs the sequence impedance model to facilitate a comparative analysis of the small-signal characteristics exhibited by GFM and GFL converters. Reference [16] constructs a comprehensive and detailed sequence impedance model of the GFM converter, encompassing the power loop and the voltage and current inner-loops. Nevertheless, there is still a lack of discussion on the small-signal characteristics of each loop. Reference [17] employs a multi-loop sequence impedance model to examine the small-signal characteristics of each control loop. However, the primary focus is on the control parameters, and the specific role of each control loop is not clearly defined. The objective of [18] and [19] is to develop an accurate model that considers the impact of frequency coupling: [18] concentrates on the sequence impedance model of the current-controlled GFM converters; whereas [19] focuses on the sequence impedance model of the voltage-controlled GFM converters. However, these models exhibit considerable degrees of complexity with dozens of dimensions when considering the frequency coupling, which presents a greater challenge for intuitive analysis of the impedance characteristics and subsequent improvement to address related small-signal instability issues. Therefore, it is imperative to simplify the model for further analysis and design.

A unified sequence impedance model is proposed to analyze the influence of different control parameters of GFM converters [20]. However, in comparison to irregular control parameters, control loops represent a more effective means of simplifying the model. Reference [21] endeavors to modularize the model of the multi-loop GFM converter into three components for further analysis. However, each component is composed of transfer function matrices, which are also too complicated to analyze. It is recommended that outer-loops and inner-loops should be modeled as interrelated components, with a view to emphasizing their respective roles in sequence impedances. Given the complexity and high dimensionality of impedance models for GFM converters, this approach can be employed for rapid modeling when the control strategy of the outer-loop or inner-loop is altered, and can also be utilized to verify the accuracy of impedance models in a timely manner.

This paper proposes a series-parallel sequence impedance model of multi-loop GFM converters to separate different control loops in GFM converters like puzzles to elucidate their physical meanings in circuits. Furthermore, this model can also be employed for rapid modeling when modifying control loops, enabling swift verification of model accuracy. Additionally, it can be utilized to elucidate the distinctive positive- and negative-sequence impedance characteristics and associated small-signal instability issues of the voltage and current inner-loops and the power outer-loop. This allows for the selection of an optimal control strategy.

Accordingly, this paper is structured as follows. Section II illustrates the process of sequence impedance modeling for GFM converters. Section III proposes the model to decompose sequence impedances into series parts and parallel parts to reveal their physical meanings in circuits. Section IV analyzes the impedance characteristics of different control loops and control parameters in GFM converters, and recommends GFM converters with the single power loop. Section V provides applications of the proposed model in addressing small-signal stability issues. Section VI employs simulations and prototype experiments to validate the findings. Section VII offers a summary of the principal contributions.

II. Sequence Impedance Modeling of GFM Converters

A. Sequence Impedance Modeling of GFM Converter with Single Power Loop

As shown in Fig. 1, a GFM converter with an ideal DC voltage source is connected to an ideal three-phase three-wire system that is three-phase symmetrical and devoid of harmonic voltages and currents.

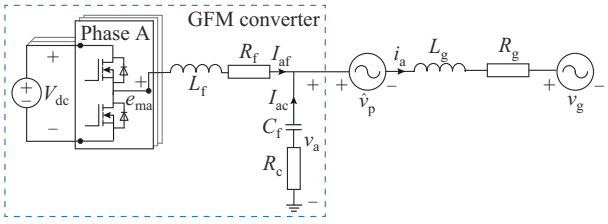

Fig. 1. Circuit model of GFM converter.

The fundamental voltage and current signals in phase A with harmonics at a certain frequency caused by disturbance or injection, i.e., $v_a(t)$ and $i_a(t)$, respectively, can be represented as two-pole frequency signals and can be expressed in the time domain as:

$$v_a(t)=V_1\cos(2\pi f_1 t)+V_p\cos(2\pi f_p t+\varphi_{vp})+V_n\cos(2\pi f_n t+\varphi_{vn}) \tag{1}$$

$$i_a(t)=I_1\cos(2\pi f_1 t+\varphi_{i1})+I_p\cos(2\pi f_p t+\varphi_{ip})+I_n\cos(2\pi f_n t+\varphi_{in}) \tag{2}$$

where V_1, V_p, and V_n are the amplitudes of the fundamental, positive-sequence, and negative-sequence voltages, respectively; I_1, I_p, and I_n are the amplitudes of the fundamental, positive-sequence, and negative-sequence currents, respectively; f_1 is the frequency of the fundamental voltage; f_p and f_n are the frequencies of the positive- and negative-sequence harmonic voltages, respectively, and $f_p=f_n$; φ_{vp} and φ_{vn} are the phase angle differences between the fundamental voltage and the positive- and negative-sequence harmonic voltages, respectively; φ_{ip} and φ_{in} are the phase angle differences between the fundamental voltage and the positive- and negative-sequence harmonic currents, respectively; and φ_{i1} is the phase angle difference between the fundamental voltage and current.

In a three-phase symmetrical system, the positive- and negative-sequence components can be decoupled [12], allowing for the discussion of the positive sequence in isolation. Real signals can be decomposed into positive- and negative-frequency values with the same amplitude, as shown in Fig. 2. This decomposition can be expressed as $\cos\omega t=(e^{j\omega t}+e^{-j\omega t})/2$.

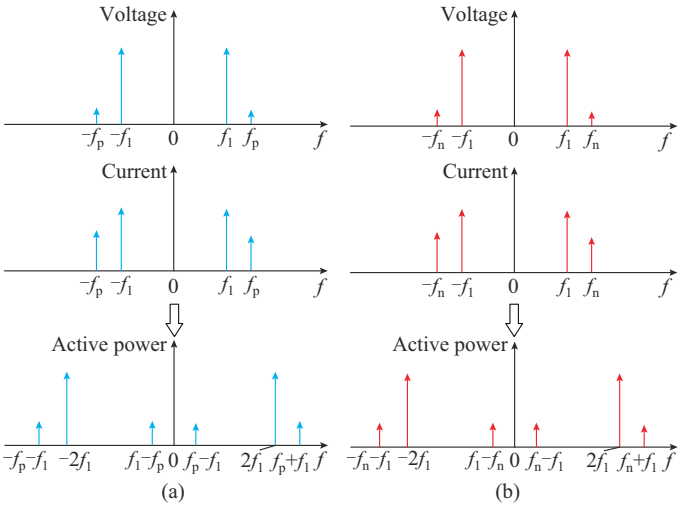

Fig. 2. Diagram of active power signals in frequency domain. (a) Positive-sequence domain. (b) Negative-sequence domain.

The voltage and current signals in the frequency domain can be expressed as (3) and (4), respectively.

$$V_a=\begin{cases}V_1/2 & f=\pm f_1\\ V_p e^{\pm j\varphi_{vp}}/2 & f=\pm f_p\end{cases} \tag{3}$$

$$I_a=\begin{cases}I_1 e^{\pm j\varphi_{i1}}/2 & f=\pm f_1\\ I_p e^{\pm j\varphi_{ip}}/2 & f=\pm f_p\end{cases} \tag{4}$$

where f is the power frequency; and the symbol ± corresponds to positive and negative frequencies.

In general, GFM converters are controlled by instantaneous power signals in the time domain, which can be obtained in the frequency domain by the frequency-domain convolution theorem. Therefore, the active power P can be obtained through the inverse Fourier transform of the product of (3) and (4) after the Fourier transform as:

$$P=\begin{cases}(V_1I_1e^{j\varphi_{i1}}+V_1I_1e^{-j\varphi_{i1}}+V_pI_pe^{j(\varphi_{vp}-\varphi_{ip})}+\\ \quad V_pI_pe^{-j(\varphi_{vp}-\varphi_{ip})})/4 & f=0\\ (V_pI_1e^{\pm j(\varphi_{vp}-\varphi_{i1})}+V_1I_pe^{\pm j\varphi_{ip}})/4 & f=\pm(f_p-f_1)\\ V_1I_1e^{\pm j\varphi_{i1}}/4 & f=\pm 2f_1\\ (V_pI_1e^{\pm j(\varphi_{vp}+\varphi_{i1})}+V_1I_pe^{\pm j\varphi_{ip}})/4 & f=\pm(f_p+f_1)\end{cases} \tag{5}$$

In a three-phase symmetrical system, the phase power can be considered in relation to the power frequency. When the power frequency is $2f_1$ or f_p+f_1 (ignoring the negative frequency), the phase power is in the positive sequence, and the sum of three-phase power is 0; when the power frequency is 0 or f_p-f_1, the phase power is in the zero sequence, and the sum of three-phase power is three times the power per phase, as given in (6). This component of active power is transferred to the DC side in accordance with the law of energy conservation.

$$P_e=\begin{cases}3(V_1I_1e^{j\varphi_{i1}}+V_1I_1e^{-j\varphi_{i1}})/4 & f=0\\ 3(V_pI_1e^{\pm j(\varphi_{vp}-\varphi_{i1})}+V_1I_pe^{\pm j\varphi_{ip}})/4 & f=\pm(f_p-f_1)\end{cases} \tag{6}$$

where P_e is the transferred active power of three-phase symmetrical system.

Similarly, the frequency f_p+f_1 caused by a negative-sequence disturbance can be transferred to the DC side and should be considered.

The control structure of GFM converter with single power loop is shown in Fig. 3.

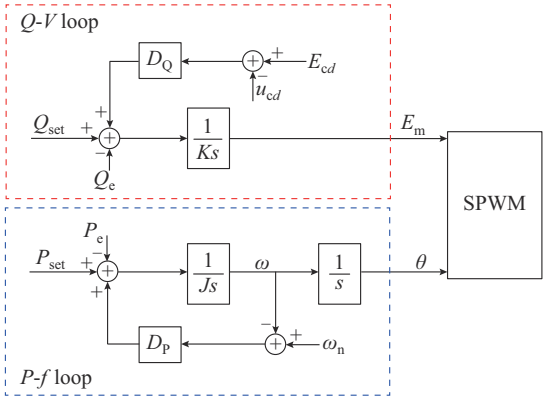

Fig. 3. Control structure of GFM converter with single power loop.

The amplitude and the phase angle of the input signal for the sinusoidal pulse width modulation (SPWM), i.e., E_m and θ, respectively, are controlled by the actual and target values of the instantaneous active and reactive power on the output side. The three-phase modulated signals e_{ma}, e_{mb}, and e_{mc} are expressed as:

$$\begin{cases}e_{ma}=E_m\cos\theta\\ e_{mb}=E_m\cos\left(\theta-\dfrac{2\pi}{3}\right)\\ e_{mc}=E_m\cos\left(\theta+\dfrac{2\pi}{3}\right)\end{cases} \tag{7}$$

In accordance with Kirchhoff's current law (KCL) and Kirchhoff's voltage law (KVL), the relationship between the terminal current and voltage of phase A in the frequency do-

main can be derived as:

$$L_{\mathrm{f}}s\left[I_{\mathrm{a}}-\frac{v_{\mathrm{a}}}{1/(C_{\mathrm{f}}s)+R_{\mathrm{c}}}\right]=e_{\mathrm{ma}}-v_{\mathrm{a}} \tag{8}$$

$$L_{\mathrm{f}}sI_{\mathrm{a}}=E_{\mathrm{m}}\cos\theta-R(s)v_{\mathrm{a}} \tag{9}$$

where L_{f} is the filtering inductance of GFM converter; C_{f} is the filtering capacitance of GFM converter; R_{c} is the equivalent resistance of C_{f}; and $R(s)=(L_{\mathrm{f}}C_{\mathrm{f}}s^2+R_{\mathrm{c}}C_{\mathrm{f}}s+1)/(R_{\mathrm{c}}C_{\mathrm{f}}s+1)$.

In accordance with (9), the sequence impedance can be determined by examining the influence of harmonics on E_{m} and θ through the implementation of control strategies.

θ can be expressed as (10) according to the *P-f* loop shown in Fig. 3.

$$\theta=\frac{1}{Js^2+D_{\mathrm{P}}s}\left(\frac{P_{\mathrm{set}}-P_{\mathrm{e}}}{\omega_{\mathrm{n}}}-D_{\mathrm{P}}\omega_{\mathrm{n}}\right) \tag{10}$$

where J and D_{P} are the virtual inertia and damping set by GFM converter, respectively; P_{set} is the setting value for the output active power of GFM converter; and ω_{n} is the rated angular velocity.

The only variable influenced by small-signal disturbances in (10) is P_{e}, which requires further research. According to (6), P_{e} can be separated into two distinct components as $P_{\mathrm{e}}=P_{\mathrm{e0}}+\Delta P_{\mathrm{e}}$, where P_{e0} is the constant fundamental active power, and ΔP_{e} is the harmonic active power. Similarly, θ can be divided as $\theta=\theta_1+\Delta\theta$, where θ_1 is the original value of phase angle, and $\Delta\theta$ is the phase angle deviation caused by the harmonic active power, which can be calculated as:

$$\Delta\theta=-\frac{\Delta P_{\mathrm{e}}}{(Js^2+D_{\mathrm{P}}s)\omega_{\mathrm{n}}} \tag{11}$$

In the frequency domain, $\Delta\theta$ can be expressed as:

$$\Delta\theta=\begin{cases}0 & f=0\\ -\dfrac{3(V_{\mathrm{p}}I_1\mathrm{e}^{\mathrm{j}\varphi_{\mathrm{vp}}}+V_1I_{\mathrm{p}}\mathrm{e}^{\mathrm{j}\varphi_{\mathrm{ip}}})}{4(Js^2+D_{\mathrm{P}}s)\omega_{\mathrm{n}}} & f=f_{\mathrm{p}}-f_1\end{cases} \tag{12}$$

Substituting $\theta=\theta_1+\Delta\theta$ into $\cos\theta$, we have:

$$\cos\theta=\cos(\theta_1+\Delta\theta)=\cos\theta_1-\Delta\theta\sin\theta_1=\frac{\mathrm{j}}{2}(\mathrm{e}^{\mathrm{j}\theta_1}-\mathrm{e}^{-\mathrm{j}\theta_1})\Delta\theta=$$
$$\frac{1}{2}(\mathrm{e}^{\mathrm{j}(\theta_1+\pi/2)}+\mathrm{e}^{-\mathrm{j}(\theta_1+\pi/2)})\Delta\theta=\frac{1}{2}(\mathrm{e}^{\mathrm{j}(\omega_{\mathrm{n}}t+\delta)}+\mathrm{e}^{-\mathrm{j}(\omega_{\mathrm{n}}t+\delta)})\Delta\theta \tag{13}$$

where $\delta=\delta_1+\pi/2$, and δ_1 is the power angle of GFM converter.

Due to the power angle characteristic of generator, we have:

$$P_{\mathrm{e}}=\frac{E_{\mathrm{m}}v_{\mathrm{a}}\sin\delta_1}{\omega_{\mathrm{n}}L_{\mathrm{f}}} \tag{14}$$

$$\delta_1=\arcsin\frac{P_{\mathrm{e}}\omega_{\mathrm{n}}L_{\mathrm{f}}}{E_{\mathrm{m}}v_{\mathrm{a}}} \tag{15}$$

Since (13) represents $\cos\theta$ in the time domain, according to (12) and the frequency-domain convolution theorem, $\cos\theta$ in the frequency domain can be derived as:

$$\cos\theta=\begin{cases}0 & f=f_1\\ -\dfrac{3\mathrm{e}^{\mathrm{j}\delta}(V_{\mathrm{p}}I_1\mathrm{e}^{\mathrm{j}\varphi_{\mathrm{vp}}}+V_1I_{\mathrm{p}}\mathrm{e}^{\mathrm{j}\varphi_{\mathrm{ip}}})}{8[J^2(s-\mathrm{j}2\pi f_1)+D_{\mathrm{P}}(s-\mathrm{j}2\pi f_1)]\omega_{\mathrm{n}}} & f=f_{\mathrm{p}}\end{cases} \tag{16}$$

Substituting (16) into (9) yields the positive-sequence impedance:

$$Z_{\mathrm{p}}(s)=-\frac{V_{\mathrm{p}}}{I_{\mathrm{p}}}\mathrm{e}^{\mathrm{j}(\varphi_{\mathrm{vp}}-\varphi_{\mathrm{ip}})}=\frac{L_{\mathrm{f}}s+\sqrt{2}\,E_{\mathrm{m}}\mathrm{e}^{\mathrm{j}\delta}M_V(s-\mathrm{j}2\pi f_1)}{R(s)+\sqrt{2}\,E_{\mathrm{m}}\mathrm{e}^{\mathrm{j}\delta}M_I(s-\mathrm{j}2\pi f_1)} \tag{17}$$

$$M_V(s)=\frac{3V_1}{4(J^2(s)+D_{\mathrm{P}}(s))\omega_{\mathrm{n}}} \tag{18}$$

$$M_I(s)=\frac{3I_1}{4(J^2(s)+D_{\mathrm{P}}(s))\omega_{\mathrm{n}}} \tag{19}$$

It is important to note that if the GFM converter is an ideal voltage source, $Z_{\mathrm{p}}(s)$ should be equal to $L_{\mathrm{f}}s/R(s)$, which is analogous to (17) particularly when $M_V(s)$ and $M_I(s)$ are relatively small.

B. Sequence Impedance Modeling of GFM Converter with Different Inner-loops

As shown in Fig. 4, multi-loop GFM converters exhibit the same power outer-loop configurations as those with single power loop. They can be classified into three categories based on their distinct inner-loops: ① single voltage loop; ② single current loop; and ③ voltage and current dual-loop.

Given that the topology of GFM converter remains unchanged, the relationship between the terminal current and voltage of phase A is analogous to (9), which can be expressed as:

$$L_{\mathrm{f}}sI_{\mathrm{a}}=e_{\mathrm{ma}}-R(s)v_{\mathrm{a}} \tag{20}$$

The modulated signal e_{ma} differs from (7) because multi-loop GFM converters employ a different SPWM. The inverse Park's transformation of (7) can be expressed as:

$$\begin{bmatrix}e_{\mathrm{ma}}\\ e_{\mathrm{mb}}\\ e_{\mathrm{mc}}\end{bmatrix}=\begin{bmatrix}\cos\theta & -\sin\theta & 1\\ -\cos\left(\theta-\dfrac{2\pi}{3}\right) & -\sin\left(\theta-\dfrac{2\pi}{3}\right) & 1\\ -\cos\left(\theta+\dfrac{2\pi}{3}\right) & -\sin\left(\theta+\dfrac{2\pi}{3}\right) & 1\end{bmatrix}\begin{bmatrix}u_d\\ u_q\\ u_0\end{bmatrix} \tag{21}$$

where u_d and u_q are the *d*- and *q*-axis voltages of modulated signals, respectively; and u_0 can be neglected in the three-phase three-wire system. e_{ma} can be derived as:

$$e_{\mathrm{ma}}=u_d\cos\theta-u_q\sin\theta \tag{22}$$

Substituting $\theta=\theta_1+\Delta\theta$ into (22), e_{ma} can be expressed as:

$$e_{\mathrm{ma}}=u_{d1}\cos\theta_1-u_{q1}\sin\theta_1 \tag{23}$$

$$u_{d1}=u_d-u_q\Delta\theta \tag{24}$$

$$u_{q1}=u_d\Delta\theta+u_q \tag{25}$$

where u_{d1} and u_{q1} are the original values for the *d*- and *q*-axis voltages of modulated signals, respectively.

u_d and u_q are determined by the inner-loops of GFM converters. As illustrated in Fig. 4, the values of u_d and u_q with different inner-loops, i.e., the single voltage loop, single current loop, and voltage and current dual-loop, can be derived as (26)-(28), respectively.

$$\begin{cases}u_d=(E-u_{cd})H_{\mathrm{v}}(s)\\ u_q=(0-u_{cq})H_{\mathrm{v}}(s)\end{cases} \tag{26}$$

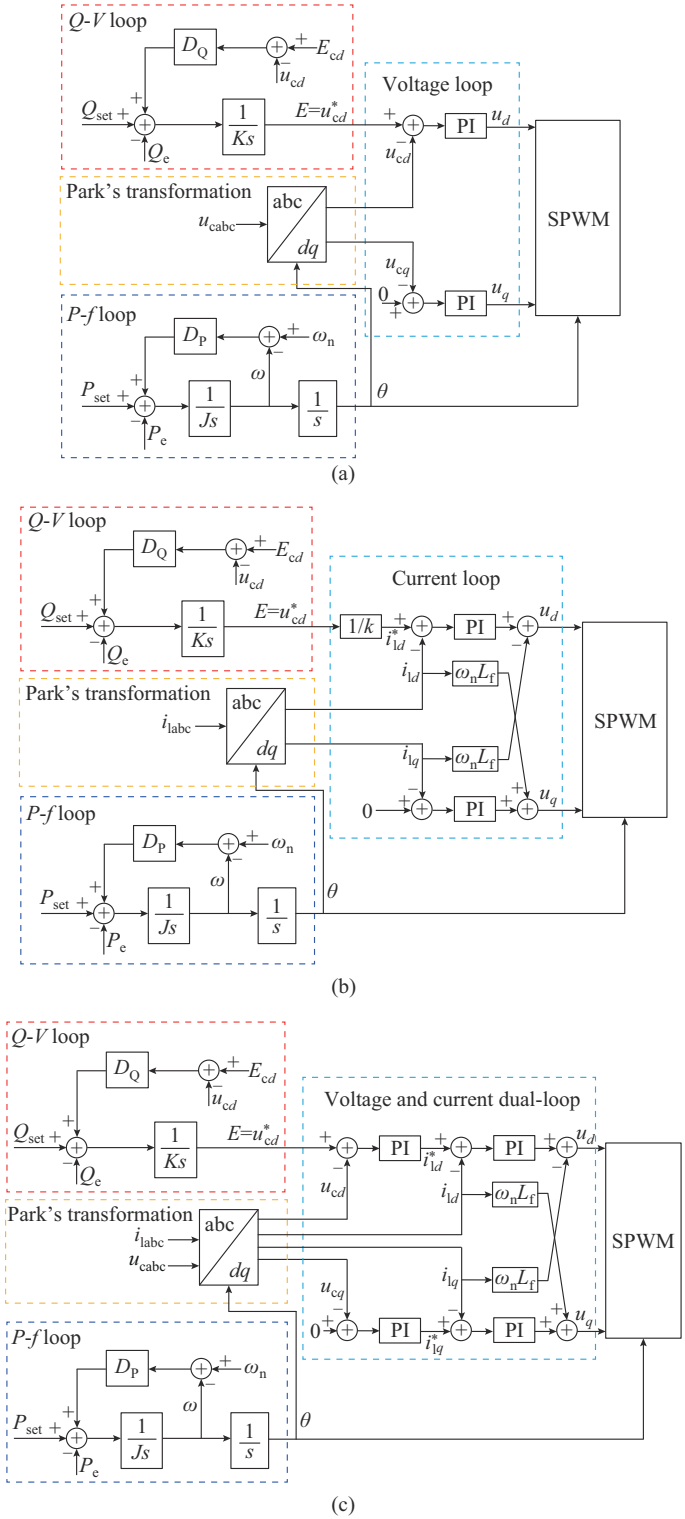

Fig. 4. Control structure of GFM converter with distinct inner-loops. (a) Single voltage loop. (b) Single current loop. (c) Voltage and current dual-loop.

$$\begin{cases} u_d=(E/k-i_{ld})H_i(s)-i_{lq}\omega_n L_f \\ u_q=(0-i_{lq})H_i(s)+i_{ld}\omega_n L_f \end{cases} \tag{27}$$

$$\begin{cases} u_d=[(E-u_{cd})H_v(s)-i_{ld}]H_i(s)-i_{lq}\omega_n L_f \\ u_q=[(0-u_{cq})H_v(s)-i_{lq}]H_i(s)+i_{ld}\omega_n L_f \end{cases} \tag{28}$$

where E is the reference voltage of modulated signals; k is the reference value of the loop impedance; u_{cd} and u_{cq} are the measured values for the d- and q-axis voltages of modulated signals, respectively; i_{ld} and i_{lq} are the measured values for the d- and q-axis currents of modulated signals, respectively; and $H_v(s)$ and $H_i(s)$ are the proportional-integral (PI) transfer functions of voltage and current loops, respectively, which can be expressed as:

$$H_v(s)=k_{vp}+\frac{k_{vi}}{s} \tag{29}$$

$$H_i(s)=k_{ip}+\frac{k_{ii}}{s} \tag{30}$$

where k_{vp} and k_{vi} are the proportional and integral parameters of voltage loop, respectively; and k_{ip} and k_{ii} are the proportional and integral parameters of current loop, respectively.

Without small-signal interferences, the actual values for the d- and q-axis voltages and the currents of modulated signals can be expressed as:

$$u_{cd1}=\begin{cases} V_1 & f=0 \\ V_p e^{j\varphi_{vp}}/2 & f=f_p-f_1 \end{cases} \tag{31}$$

$$u_{cq1}=\begin{cases} 0 & f=0 \\ -jV_p e^{j\varphi_{vp}}/2 & f=f_p-f_1 \end{cases} \tag{32}$$

$$i_{ld1}=\begin{cases} I_1 & f=0 \\ I_p e^{j\varphi_{ip}}/2 & f=f_p-f_1 \end{cases} \tag{33}$$

$$i_{lq1}=\begin{cases} 0 & f=0 \\ -jI_p e^{j\varphi_{ip}}/2 & f=f_p-f_1 \end{cases} \tag{34}$$

Considering the impact of small-signal interference on the Park's transformation through θ, the measured values of d- and q-axis voltages of modulated signals can be derived as:

$$\begin{bmatrix} u_{cd} \\ u_{cq} \\ u_0 \end{bmatrix}=\boldsymbol{T}(\theta)\begin{bmatrix} e_{ma} \\ e_{mb} \\ e_{mc} \end{bmatrix}=\begin{bmatrix} 1 & \Delta\theta & 0 \\ -\Delta\theta & 1 & 0 \\ 0 & 0 & 1 \end{bmatrix}\begin{bmatrix} u_{cd1} \\ u_{cq1} \\ u_0 \end{bmatrix} \tag{35}$$

$$\boldsymbol{T}(\theta)=\begin{bmatrix} \frac{2}{3}\cos\theta & \frac{2}{3}\cos\left(\theta-\frac{2\pi}{3}\right) & \frac{2}{3}\cos\left(\theta+\frac{2\pi}{3}\right) \\ -\frac{2}{3}\sin\theta & -\frac{2}{3}\sin\left(\theta-\frac{2\pi}{3}\right) & -\frac{2}{3}\sin\left(\theta+\frac{2\pi}{3}\right) \\ \frac{1}{3} & \frac{1}{3} & \frac{1}{3} \end{bmatrix} \tag{36}$$

Therefore, the measured values for the d- and q-axis voltages and currents of modulated signals considering the small-signal interference can be expressed as:

$$\begin{cases} u_{cd}=u_{cd1}+\Delta\theta u_{cq1} \\ u_{cq}=-\Delta\theta u_{cd1}+u_{cq1} \end{cases} \tag{37}$$

$$\begin{cases} i_{ld}=i_{ld1}+\Delta\theta i_{lq1} \\ i_{lq}=-\Delta\theta i_{ld1}+i_{lq1} \end{cases} \tag{38}$$

Substituting (31) to (35) and (12) into (37) and (38), we have:

$$u_{cd}=\begin{cases}V_1 & f=0\\ V_{\mathrm{p}}\mathrm{e}^{\mathrm{j}\varphi_{\mathrm{vp}}}/2 & f=f_{\mathrm{p}}-f_1\end{cases} \tag{39}$$

$$u_{cq}=\begin{cases}0 & f=0\\ \dfrac{3(V_{\mathrm{p}}I_1\mathrm{e}^{\mathrm{j}\varphi_{\mathrm{vp}}}+V_1I_{\mathrm{p}}\mathrm{e}^{\mathrm{j}\varphi_{\mathrm{ip}}})}{4(Js^2+D_{\mathrm{P}}s)\omega_{\mathrm{n}}}V_1-\dfrac{\mathrm{j}V_{\mathrm{p}}\mathrm{e}^{\mathrm{j}\varphi_{\mathrm{vp}}}}{2} & f=f_{\mathrm{p}}-f_1\end{cases} \tag{40}$$

$$i_{ld}=\begin{cases}I_1 & f=0\\ I_{\mathrm{p}}\mathrm{e}^{\mathrm{j}\varphi_{\mathrm{ip}}}/2 & f=f_{\mathrm{p}}-f_1\end{cases} \tag{41}$$

$$i_{lq}=\begin{cases}0 & f=0\\ \dfrac{3(V_{\mathrm{p}}I_1\mathrm{e}^{\mathrm{j}\varphi_{\mathrm{vp}}}+V_1I_{\mathrm{p}}\mathrm{e}^{\mathrm{j}\varphi_{\mathrm{ip}}})}{4(Js^2+D_{\mathrm{P}}s)\omega_{\mathrm{n}}}I_1-\dfrac{\mathrm{j}I_{\mathrm{p}}\mathrm{e}^{\mathrm{j}\varphi_{\mathrm{ip}}}}{2} & f=f_{\mathrm{p}}-f_1\end{cases} \tag{42}$$

Substituting (39) - (42) into (26) - (28), and according to (20) and (22), the positive-sequence impedances of GFM converter with single voltage loop, single current loop, and voltage and current dual-loop, i.e., $Z_{\mathrm{VP}}(s)$, $Z_{\mathrm{IP}}(s)$, and $Z_{\mathrm{VIP}}(s)$, respectively, can be derived as (43)-(45).

$$Z_{\mathrm{VP}}(s)=\frac{L_{\mathrm{f}}s+K_{\mathrm{pwm}}V_{\mathrm{dc}}\mathrm{e}^{\mathrm{j}\delta}M_V(s-\mathrm{j}\omega_{\mathrm{n}})V_1H_{\mathrm{v}}(s-\mathrm{j}\omega_{\mathrm{n}})}{R(s)+K_{\mathrm{pwm}}V_{\mathrm{dc}}V_1M_I(s-\mathrm{j}\omega_{\mathrm{n}})H_{\mathrm{v}}(s-\mathrm{j}\omega_{\mathrm{n}})-\mathrm{j}\mathrm{e}^{\mathrm{j}\delta}K_{\mathrm{pwm}}V_{\mathrm{dc}}H_{\mathrm{v}}(s-\mathrm{j}\omega_{\mathrm{n}})} \tag{43}$$

$$Z_{\mathrm{IP}}(s)=\frac{L_{\mathrm{f}}s+K_{\mathrm{pwm}}V_{\mathrm{dc}}\mathrm{e}^{\mathrm{j}\delta}\dfrac{E}{k}M_V(s-\mathrm{j}\omega_{\mathrm{n}})H_{\mathrm{i}}(s-\mathrm{j}\omega_{\mathrm{n}})-\mathrm{j}K_{\mathrm{pwm}}V_{\mathrm{dc}}\mathrm{e}^{\mathrm{j}\delta}H_{\mathrm{v}}(s-\mathrm{j}\omega_{\mathrm{n}})}{R(s)+K_{\mathrm{pwm}}V_{\mathrm{dc}}\mathrm{e}^{\mathrm{j}\delta}\dfrac{E}{k}M_I(s-\mathrm{j}\omega_{\mathrm{n}})H_{\mathrm{i}}(s-\mathrm{j}\omega_{\mathrm{n}})} \tag{44}$$

$$Z_{\mathrm{IVP}}(s)=\frac{L_{\mathrm{f}}s+K_{\mathrm{pwm}}V_{\mathrm{dc}}V_1\mathrm{e}^{\mathrm{j}\delta}M_V(s-\mathrm{j}\omega_{\mathrm{n}})H_{\mathrm{vi}}(s-\mathrm{j}\omega_{\mathrm{n}})-\mathrm{j}K_{\mathrm{pwm}}V_{\mathrm{dc}}\mathrm{e}^{\mathrm{j}\delta}(H_{\mathrm{i}}(s-\mathrm{j}\omega_{\mathrm{n}})-\mathrm{j}\omega_{\mathrm{n}}L_{\mathrm{f}})}{R(s)+K_{\mathrm{pwm}}V_{\mathrm{dc}}V_1\mathrm{e}^{\mathrm{j}\delta}M_I(s-\mathrm{j}\omega_{\mathrm{n}})H_{\mathrm{vi}}(s-\mathrm{j}\omega_{\mathrm{n}})-\mathrm{j}K_{\mathrm{pwm}}V_{\mathrm{dc}}\mathrm{e}^{\mathrm{j}\delta}H_{\mathrm{vi}}(s-\mathrm{j}\omega_{\mathrm{n}})} \tag{45}$$

where K_{pwm} is the modulation ratio of GFM converter; $H_{\mathrm{vi}}(s)$ is the PI transfer function of voltage and current dual-loop; and V_{dc} is the DC-side voltage.

III. Derivation of Series-parallel Sequence Impedance Model of Multi-loop GFM Converters

A. Model Decomposing

The all-in-one impedance model, as shown in (43) - (45), appears to be overly intricate for the analysis of small-signal characteristics. Accordingly, this paper proposes a series-parallel sequence impedance model of multi-loop GFM converters to reveal the interrelationship between characteristics from a physical standpoint. An examination of (43) - (45) reveals that the numerators and denominators exhibit analogous components. The numerators can be partitioned into two parts based on the plus sign, whereas the denominators cannot. The denominators can be transformed into the numerators through the reciprocal change, and then can be split into two parts. Therefore, (46) and (47) can be derived from (43) and (45), respectively.

$$\frac{1}{Z_{\mathrm{VP}}(s)}=\frac{R(s)+K_{\mathrm{pwm}}V_{\mathrm{dc}}V_1M_I(s-\mathrm{j}\omega_{\mathrm{n}})H_{\mathrm{v}}(s-\mathrm{j}\omega_{\mathrm{n}})-\mathrm{j}K_{\mathrm{pwm}}V_{\mathrm{dc}}\mathrm{e}^{\mathrm{j}\delta}H_{\mathrm{v}}(s-\mathrm{j}\omega_{\mathrm{n}})}{L_{\mathrm{f}}s+K_{\mathrm{pwm}}V_{\mathrm{dc}}\mathrm{e}^{\mathrm{j}\delta}M_V(s-\mathrm{j}\omega_{\mathrm{n}})V_1H_{\mathrm{v}}(\mathrm{s}-\mathrm{j}\omega_{\mathrm{n}})} \tag{46}$$

$$\begin{aligned}\frac{1}{Z_{\mathrm{IVP}}(s)}=&\frac{R(s)+K_{\mathrm{pwm}}V_{\mathrm{dc}}V_1\mathrm{e}^{\mathrm{j}\delta}M_I(s-\mathrm{j}\omega_{\mathrm{n}})H_{\mathrm{vi}}(s-\mathrm{j}\omega_{\mathrm{n}})-\mathrm{j}K_{\mathrm{pwm}}V_{\mathrm{dc}}\mathrm{e}^{\mathrm{j}\delta}H_{\mathrm{vi}}(s-\mathrm{j}\omega_{\mathrm{n}})}{L_{\mathrm{f}}s+K_{\mathrm{pwm}}V_{\mathrm{dc}}V_1\mathrm{e}^{\mathrm{j}\delta}M_V(s-\mathrm{j}\omega_{\mathrm{n}})H_{\mathrm{vi}}(s-\mathrm{j}\omega_{\mathrm{n}})-\mathrm{j}K_{\mathrm{pwm}}V_{\mathrm{dc}}\mathrm{e}^{\mathrm{j}\delta}(H_{\mathrm{i}}(s-\mathrm{j}\omega_{\mathrm{n}})-\mathrm{j}\omega_{\mathrm{n}}L_{\mathrm{f}})}=\\ &\frac{R(s)+K_{\mathrm{pwm}}V_{\mathrm{dc}}V_1\mathrm{e}^{\mathrm{j}\delta}M_I(s-\mathrm{j}\omega_{\mathrm{n}})H_{\mathrm{vi}}(s-\mathrm{j}\omega_{\mathrm{n}})}{L_{\mathrm{f}}s+K_{\mathrm{pwm}}V_{\mathrm{dc}}V_1\mathrm{e}^{\mathrm{j}\delta}M_V(s-\mathrm{j}\omega_{\mathrm{n}})H_{\mathrm{vi}}(s-\mathrm{j}\omega_{\mathrm{n}})-\mathrm{j}K_{\mathrm{pwm}}V_{\mathrm{dc}}\mathrm{e}^{\mathrm{j}\delta}(H_{\mathrm{i}}(\mathrm{s}-\mathrm{j}\omega_{\mathrm{n}})-\mathrm{j}\omega_{\mathrm{n}}L_{\mathrm{f}})}+\\ &\frac{-\mathrm{j}K_{\mathrm{pwm}}V_{\mathrm{dc}}\mathrm{e}^{\mathrm{j}\delta}H_{\mathrm{vi}}(\mathrm{s}-\mathrm{j}\omega_{\mathrm{n}})}{L_{\mathrm{f}}s+K_{\mathrm{pwm}}V_{\mathrm{dc}}V_1\mathrm{e}^{\mathrm{j}\delta}M_V(s-\mathrm{j}\omega_{\mathrm{n}})H_{\mathrm{vi}}(s-\mathrm{j}\omega_{\mathrm{n}})-\mathrm{j}K_{\mathrm{pwm}}V_{\mathrm{dc}}\mathrm{e}^{\mathrm{j}\delta}(H_{\mathrm{i}}(s-\mathrm{j}\omega_{\mathrm{n}})-\mathrm{j}\omega_{\mathrm{n}}L_{\mathrm{f}})}\end{aligned} \tag{47}$$

To simplify the form, (48)-(50) can be derived from (44), (46), and (47), respectively.

$$\frac{1}{Z_{\mathrm{VP}}(s)}=Y_{\mathrm{VP,C}}(s)+Y_{\mathrm{VP,par}}(s) \tag{48}$$

$$Z_{\mathrm{IP}}(s)=Z_{\mathrm{IP,C}}(s)+Z_{\mathrm{IP,ser}}(s) \tag{49}$$

$$\frac{1}{Z_{\mathrm{IVP}}(s)}=\frac{1}{Z_{\mathrm{IVP,C}}(s)+Z_{\mathrm{IVP,ser1}}(s)}+\frac{1}{Z_{\mathrm{IVP,parC}}(s)+Z_{\mathrm{IVP,par1}}(s)} \tag{50}$$

where

$$\frac{1}{Y_{\mathrm{VP,C}}(s)}=\frac{L_{\mathrm{f}}s+K_{\mathrm{VP}}\mathrm{e}^{\mathrm{j}\delta}M_V(s-\mathrm{j}\omega_{\mathrm{n}})H_{\mathrm{v}}(s-\mathrm{j}\omega_{\mathrm{n}})}{R(s)+K_{\mathrm{VP}}\mathrm{e}^{\mathrm{j}\delta}M_I(s-\mathrm{j}\omega_{\mathrm{n}})H_{\mathrm{v}}(s-\mathrm{j}\omega_{\mathrm{n}})} \tag{51}$$

$$Y_{\mathrm{VP,par}}(s)=\frac{-\mathrm{j}\mathrm{e}^{\mathrm{j}\delta}(K_{\mathrm{VP}}/V_1)H_{\mathrm{v}}(s-\mathrm{j}\omega_{\mathrm{n}})}{L_{\mathrm{f}}s+K_{\mathrm{VP}}\mathrm{e}^{\mathrm{j}\delta}M_V(s-\mathrm{j}\omega_{\mathrm{n}})H_{\mathrm{v}}(s-\mathrm{j}\omega_{\mathrm{n}})} \tag{52}$$

$$Z_{\mathrm{IP,C}}(s)=\frac{L_{\mathrm{f}}s+K_{\mathrm{IP}}\mathrm{e}^{\mathrm{j}\delta}M_V(s-\mathrm{j}\omega_{\mathrm{n}})H_{\mathrm{i}}(\mathrm{s}-\mathrm{j}\omega_{\mathrm{n}})}{R(s)+K_{\mathrm{IP}}\mathrm{e}^{\mathrm{j}\delta}M_I(\mathrm{s}-\mathrm{j}\omega_{\mathrm{n}})H_{\mathrm{i}}(\mathrm{s}-\mathrm{j}\omega_{\mathrm{n}})} \tag{53}$$

$$Z_{\mathrm{IP,ser}}(s)=\frac{-\mathrm{j}\mathrm{e}^{\mathrm{j}\delta}(K_{\mathrm{VP}}/I_1)(H_{\mathrm{i}}(s-\mathrm{j}\omega_{\mathrm{n}})-\mathrm{j}\omega_{\mathrm{n}}L_{\mathrm{f}})}{R(s)+K_{\mathrm{VP}}\mathrm{e}^{\mathrm{j}\delta}M_I(s-\mathrm{j}\omega_{\mathrm{n}})H_{\mathrm{i}}(s-\mathrm{j}\omega_{\mathrm{n}})} \tag{54}$$

$$Z_{\mathrm{IVP,C}}(s)=\frac{L_{\mathrm{f}}s+K_{\mathrm{IVP}}\mathrm{e}^{\mathrm{j}\delta}M_V(s-\mathrm{j}\omega_{\mathrm{n}})H_{\mathrm{vi}}(s-\mathrm{j}\omega_{\mathrm{n}})}{R(s)+K_{\mathrm{IVP}}\mathrm{e}^{\mathrm{j}\delta}M_I(s-\mathrm{j}\omega_{\mathrm{n}})H_{\mathrm{vi}}(s-\mathrm{j}\omega_{\mathrm{n}})} \tag{55}$$

$$Z_{\mathrm{IVP,ser1}}(s)=\frac{-\mathrm{j}\mathrm{e}^{\mathrm{j}\delta}(K_{\mathrm{IVP}}/V_1)(H_{\mathrm{i}}(s-\mathrm{j}\omega_{\mathrm{n}})-\mathrm{j}\omega_{\mathrm{n}}L_{\mathrm{f}})}{R(s)+K_{\mathrm{IVP}}\mathrm{e}^{\mathrm{j}\delta}M_I(s-\mathrm{j}\omega_{\mathrm{n}})H_{\mathrm{vi}}(s-\mathrm{j}\omega_{\mathrm{n}})} \tag{56}$$

$$\frac{1}{Z_{\mathrm{IVP,parC}}(s)}=\frac{-\mathrm{j}\mathrm{e}^{\mathrm{j}\delta}(K_{\mathrm{IVP}}/V_1)H_{\mathrm{vi}}(s-\mathrm{j}\omega_{\mathrm{n}})}{L_{\mathrm{f}}s+K_{\mathrm{IVP}}\mathrm{e}^{\mathrm{j}\delta}M_{\mathrm{V}}(s-\mathrm{j}\omega_1)H_{\mathrm{vi}}(s-\mathrm{j}\omega_{\mathrm{n}})} \tag{57}$$

$$\frac{1}{Z_{\mathrm{IVP,par1}}(s)}=\frac{-\mathrm{j}\mathrm{e}^{\mathrm{j}\delta}(K_{\mathrm{IVP}}/V_1)\mathrm{e}^{\mathrm{j}\delta}H_{\mathrm{vi}}(s-\mathrm{j}\omega_{\mathrm{n}})}{-\mathrm{j}(K_{\mathrm{IVP}}/V_1)\mathrm{e}^{\mathrm{j}\delta}(H_{\mathrm{i}}(s-\mathrm{j}\omega_{\mathrm{n}})-\mathrm{j}\omega_{\mathrm{n}}L_{\mathrm{f}})} \tag{58}$$

where $K_{VP}=K_{IVP}=K_{pwm}V_{dc}V_1$; and $K_{IP}=K_{pwm}V_{dc}E/k$.

In a physical sense, given that (51)-(58) all represent impedance, the splitting terms of the numerators can be regarded as impedances in series, and the splitting terms of the denominators can be regarded as admittance in series, i.e., impedances in parallel.

As shown in (48)-(50), the positive-sequence impedance of the GFM converter with a single voltage loop can be conceptualized as two impedances in parallel. Similarly, the positive-sequence impedances of GFM converters with a single current loop can be conceptualized as two impedances in series. Furthermore, the positive-sequence impedances of GFM converters with voltage and current dual-loop can be seen as two impedances in parallel, where each impedance can be viewed as two impedances in series.

Additionally, (51), (53), and (55) exhibit analogous forms to (17), i.e., the impedance of GFM converter with the single power loop. They share: ① a common filter component and power loop component, i.e., $L_f s/R(s)$ and $M_V(s-j\omega_n)/M_I(s-j\omega_n)$, respectively; ② the constant component, i.e., $\sqrt{2}E_m$ for the single power loop, K_{VP} for the single voltage loop, K_{IVP} for the voltage and current dual-loop, and K_{IP} for the single current loop; and ③ the PI controller component, i.e., $H_v(s-j\omega_n)$ for the single voltage loop, $H_i(s-j\omega_n)$ for the single current loop, and $H_{vi}(s-j\omega_n)$ for the voltage and current dual-loop. Similarly, a comparison of (52) and (57), or (54) and (56), reveals that they exhibit similar forms, which can be classified as series impedances and parallel impedances, respectively. Therefore, it can be concluded that, in GFM converters, the voltage loop acts as a parallel impedance, while the current loop acts as a series impedance.

Additionally, two more points of interest regarding the positive-sequence impedances of GFM converters warrant consideration. One noteworthy point is that the positive-sequence impedances maintain coupling terms. The coupling term $j\omega_n L_f$ in the current loop results in the appearance of additional coupling terms such as $H_v(s-j\omega_n)$ in both the numerator and the denominator due to the frequency-domain convolution calculation. This leads to the positive-sequence impedance being nearly infinite around the fundamental frequency. Another point is that $-je^{j\delta}$ appears in each numerator of the series and parallel components, indicating that the voltage and current loops exhibit similar capacitive resistance characteristics. However, these intriguing observations do not fully capture the true nature of GFM converters. To gain a more comprehensive understanding and to further apply the proposed model in small-signal analysis, it is essential to analyze the proposed model through corresponding schematic diagrams and Bode diagrams.

B. Model Complexity and Computational Efficiency

Given that each circuit element is composed of resistance, capacitance, and inductance, which can be represented by no more than three dimensions, the proposed model of GFM converter with voltage and current dual-loop, which comprises four elements, can be considered to have less than 12 dimensions. This is a considerably more compact representation than those presented in [18] and [19], which encompass over 20 dimensions. Moreover, as each element can be examined separately, the proposed model can be regarded as having only three dimensions. The low dimensionality of the proposed model results in a considerable increase in computational efficiency. The proposed model can be calculated over 100000 sampling points in the Bode diagram, ranging from 1 Hz to 100 kHz, in less than 0.3 s. This capability enables the rapid analysis of the small-signal characteristics of GFM converter.

IV. Impedance Characteristics of GFM converter with Different Control Loops

A. Positive-sequence Impedances of GFM Converter with Different Control Loops

The system parameters of GFM converter with different control loops are shown in Table I, where L_g is the equivalent inductance of grid; R_g is the equivalent resistance of grid; and Q_{set} is the setting value for output reactive power of GFM converter. Figure 5 shows the Bode diagram for positive-sequence impedances of GFM converters with different control loops, where blue lines are theoretical results derived from (17) and (43)-(45), and red circles are derived from the corresponding frequency-sweep simulations based on RT-Box shown in Fig. 6. The discrepancy between the theoretical and simulation results can be attributed to the phenomenon of frequency coupling, which arises from the conversion of active power on the AC and DC sides [18], [19]. As shown in Fig. 5, the frequency coupling phenomenon exerts a negligible influence on the amplitude and phase of positive-sequence impedances and does not alter the series and parallel composition of each control loop in the proposed model. Consequently, it can be disregarded to streamline the sequence impedances and corresponding stability analysis.

TABLE I
System Parameters of GFM Converters

Parameter	Value	Parameter	Value
ω_n (rad·s)	100π	D_P (N·s/m)	20
P_{set} (kW)	10	J (kg·m^2)	0.05
Q_{set} (kVA)	0	k_{vp}	0.2
V_1 (V)	311.13	k_{vi}	20
V_{dc} (V)	690	k_{ip}	1
I_1 (A)	10.71	k_{ii}	5
L_f (mH)	3.2	R_f (Ω)	1.5
C_f (μF)	20	R_g (Ω)	0.1
L_g (mH)	3.2		

By comparing the distinction between the amplitude and phase of impedances at low and high frequencies (where the dividing line is twice the fundamental frequency [13], [22]), it is possible to divide the positive-sequence impedance of GFM converters into two groups based on the presence or absence of the current loop in the control strategy. For GFM converters utilizing the single power loop or the single volt-

age loop, which lack the current loop, they exhibit inductive output impedance at low frequencies. Conversely, for GFM converters utilizing the single current loop or the voltage and current dual-loop, they exhibit capacitive output impedance at low frequencies.

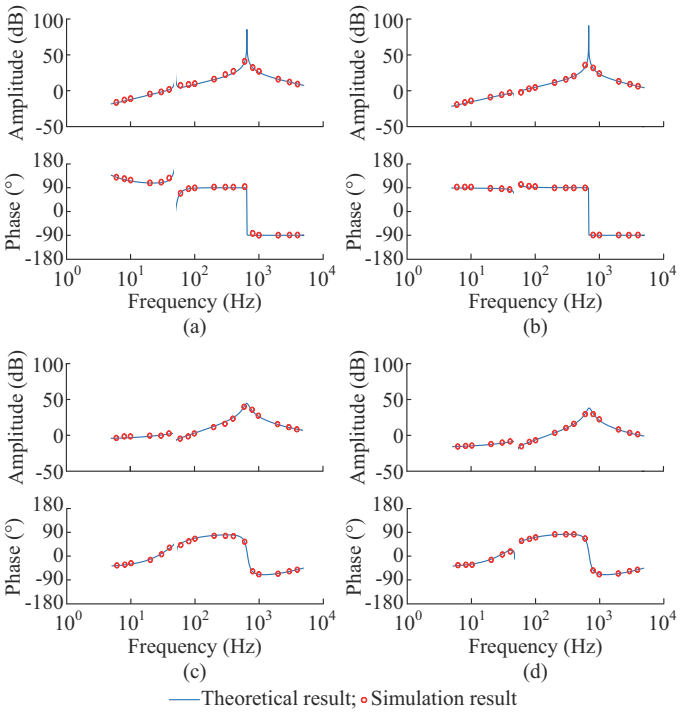

Fig. 5. Bode diagram for positive-sequence impedance of GFM converter with different control loops. (a) Single power loop. (b) Single voltage loop. (c) Single current loop. (d) Voltage and current dual-loop.

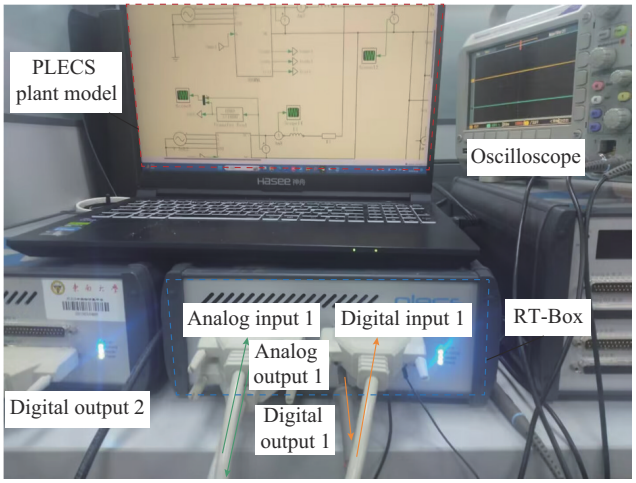

Fig. 6. RT-Box experiment platform.

From the standpoint of quantitative analysis, the stability margins with different control loops are shown in Supplementary Material A Table SAI and Fig. SA1.

In general, the grid impedance connected with the GFM converter exhibits inductive characteristics, which indicates that the sum of capacitive output impedances of GFM converter and the inductive grid impedance may be close to zero, thereby causing instability. Therefore, the current loop is of significance as a series component in modifying low-frequency impedance characteristics.

The above low-frequency positive-sequence impedance characteristics can also be derived from the proposed model. As previously stated, the proposed model of GFM converter includes a low-frequency inductive impedance due to the inductive component $L_f s/R(s)$ in (17), (51), (53), and (55). In the proposed model of GFM converter with either a single voltage loop or a single current loop, the components expressed as (52) and (54) are included, which have a similar capacitive impedance and are used to reduce the inductance component and increase the capacitive component. This is achieved by the capacitive component $-je^{j\delta}$ in the numerator and the inductive component $L_f s$ or the resistor-inductance component $R(s)$ in the denominator. Nevertheless, (52) behaves as a parallel impedance while (54) behaves as a series one. In general, the parallel impedance caused by the voltage loop will reduce the amplitude, whereas the series impedance caused by the current loop will increase the amplitude. Since the inductive impedance resulting from the power loop has a relatively small amplitude at low frequencies, the decreasing effect of the voltage loop on the impedance amplitude of the power loop is considerably less than the increasing effect of the current loop. Therefore, the voltage loop appears to be inconsequential as a series component in altering low-frequency impedance characteristics.

At high frequencies, however, the GFM converters with different control loops exhibit similar capacitive impedance characteristics with relatively high amplitude, as shown in Fig. 5. This is because the parallel component resulting from the voltage loop has a relatively large amplitude, while the series component resulting from the current loop has a relatively small amplitude. Both have a negligible effect on the high-amplitude capacitive impedance resulting from the power loop. Because of the parallel resonance, the impedance is infinite around the resonance frequency of LC filter f_{LC}, as expressed in (59). Consequently, the positive-sequence impedances of GFM converters and the grid with a 180° phase shift must have an intersection frequency in the Bode diagram higher than the resonance frequency with various values of short-circuit ratio (SCR), which can be calculated as (60) to measure the grid strength [23], [24], as shown in Fig. 7.

$$f_{LC} = \frac{2\pi}{\sqrt{L_g C_f}} \tag{59}$$

$$SCR = \frac{P_{sc}}{P_N} = \frac{3U_a^2}{Z_g P_{set}} \tag{60}$$

where P_{sc} is the short-circuit capacity of grid; U_a is the effective value of v_a; Z_g is the equivalent impedance of grid; and P_N is the rated active transmission power of GFM converter.

This indicates that the GFM converter with distinct voltage or current loops exhibits similar small-signal instability issues at high frequencies. Therefore, the impact of different control loops should be concentrated more at low frequencies. Previous results derived from the proposed model and corresponding Bode diagrams indicate that the single power loop is the preferred option due to fewer parameters in-

volved, which makes control easier and provides prior small-signal stability at low frequency. Furthermore, the single power loop can control the inner electric potential by its amplitude E and phase δ instead of u_d and u_q, which can provide more stable voltage support during instability.

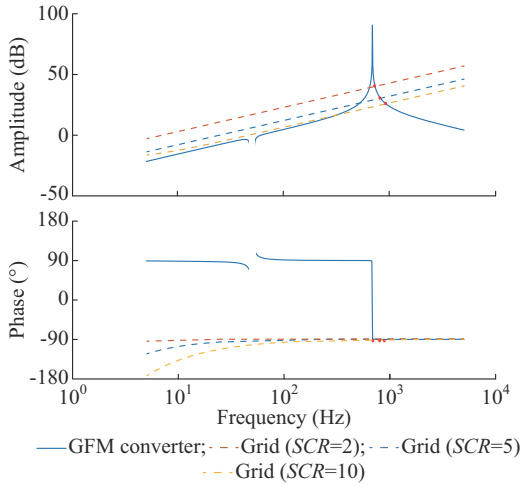

Fig. 7. Bode diagram of positive-sequence impedances of GFM converter and grid with 180° phase shift.

B. Negative-sequence Impedances of Different Control Loops

In general, the negative-sequence impedances exhibit fewer characteristics [15], [25], and the negative-sequence impedances of GFM converters with various control loops have similar amplitudes and phases. The Bode diagrams of the negative-sequence impedances of GFM converters with four control loops are shown in Supplementary Material A Fig. SA2.

C. Influences of Control Parameters

The influences of control parameters J, D_{p}, k_{vp}, and k_{vi} on positive-sequence impedance of GFM converters are shown in Fig. 8. It can be concluded that J and D_{p} exert their main influences mainly at low frequencies, whereas the PI parameters k_{vp} and k_{vi} exert influence at both low frequencies around 50 Hz and high frequencies around f_{LC}. According to the proposed model, the aforementioned phenomenon can be elucidated by the assertion that the impedance component determined by J and D_{p} is also in series with $L_{\mathrm{f}}s$. $L_{\mathrm{f}}s$ exhibits a high amplitude at high frequencies, thereby reducing the influences of J and D_{p}.

A sensitivity analysis can offer valuable insights into the robustness of the proposed model under different parameters. Therefore, the parameter-based sensitivity analysis method introduced in [26] can be employed, which is expressed as:

$$S_{\mathrm{para}} = \frac{\partial P_M}{\partial p_{ara}} \approx \frac{P_M(p_{ara0}+\Delta p_{ara}) - P_M(p_{ara0})}{\Delta p_{ara}} \tag{61}$$

where S_{para} is the sensitivity of each parameter; P_M is the phase margin of GFM converter; p_{ara} represents various control parameters such as J, D_{p}, k_{vp}, k_{vi}; p_{ara0} is the original value of each control parameter; and $\Delta p_{ara} = 0.1\, p_{ara0}$ is the parameter perturbation.

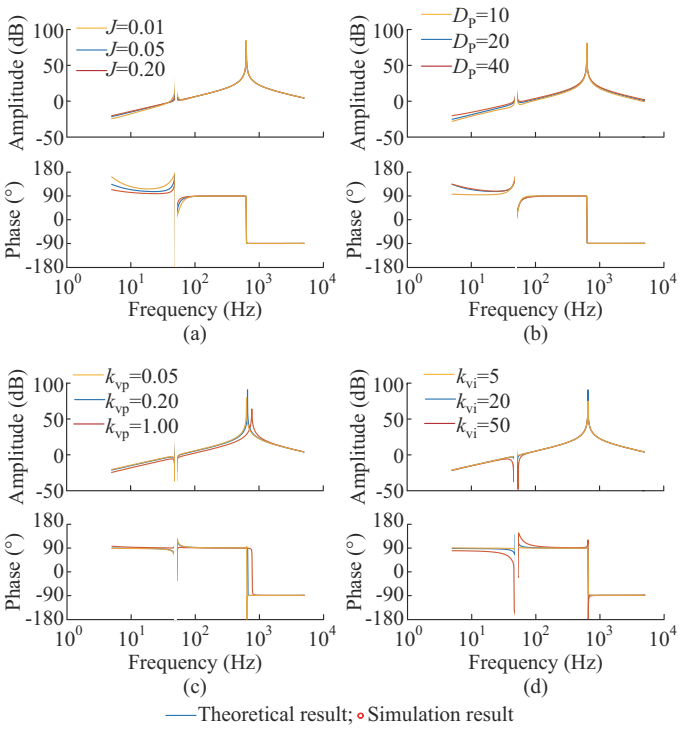

Fig. 8. Influences of control parameters on positive-sequence impedance of GFM converters. (a) J. (b) D_{p}. (c) k_{vp}. (d) k_{vi}.

The parameter-based sensitivity analysis results can be obtained in Table II. It can be observed that the small-signal instability is predominantly associated with control parameters J and D_{p}. However, a comparison between Fig. 5 and Fig. 8 reveals that the impact of parameter alterations on positive-sequence impedance characteristics is relatively insignificant in comparison to the influence of control loops.

TABLE II
PARAMETER-BASED SENSITIVITY ANALYSIS RESULTS

Control parameter	S_{para}
J	−5.7
D_{p}	0.3
k_{vp}	0.1
k_{vi}	−0.1

As shown in Table III, the phase and amplitude characteristics of different control loops and parameters in the proposed model are summarized.

V. APPLICATION OF SERIES-PARALLEL SEQUENCE IMPEDANCE MODEL IN SMALL-SIGNAL ANALYSIS

The impedance analysis in Section III indicates that the proposed model can be effectively employed to analyze and modify the small-signal stability of GFM converters with high speed and efficacy. However, the aforementioned improvement is limited in scope. It is more beneficial to equip people with the knowledge to conduct further research than to conduct the results for them. Therefore, it is necessary to restate how to use the proposed model to improve the small-signal stability characteristics.

TABLE III
PHASE AND AMPLITUDE CHARACTERISTICS

Impedance model	Control loop and parameter	Characteristic	
		Low-frequency	High-frequency
Positive-sequence	Power loop	Inductive, small-amplitude	*Capacitive, *high-amplitude
	Voltage loop (parallel)	Capacitive, high-amplitude	Capacitive, high-amplitude
	Current loop (series)	*Capacitive, *high-amplitude	Capacitive, small-amplitude
	J (series)	Capacitive, small-amplitude	Inductive, small-amplitude
	D_p (series)	Inductive, small-amplitude	Capacitive, small-amplitude
	k_{vp} (parallel)	Inductive, high-amplitude	Capacitive, high-amplitude
	k_{vi} (parallel)	Capacitive, high-amplitude	Inductive, high-amplitude
Negative-sequence	Power loop	Inductive, small-amplitude	*Capacitive, *high-amplitude
	Voltage loop (parallel)	Capacitive, high-amplitude	Capacitive, high-amplitude
	Current loop (series)	Capacitive, small-amplitude	Capacitive, small-amplitude

Note: * means the corresponding loop plays a leading role in the proposed model.

As shown in Fig. 9, the positive-sequence impedances of GFM converters with different control loops are partitioned into disparate circuit elements in series or in parallel. Different colors are used to indicate various elements determined by different control loops.

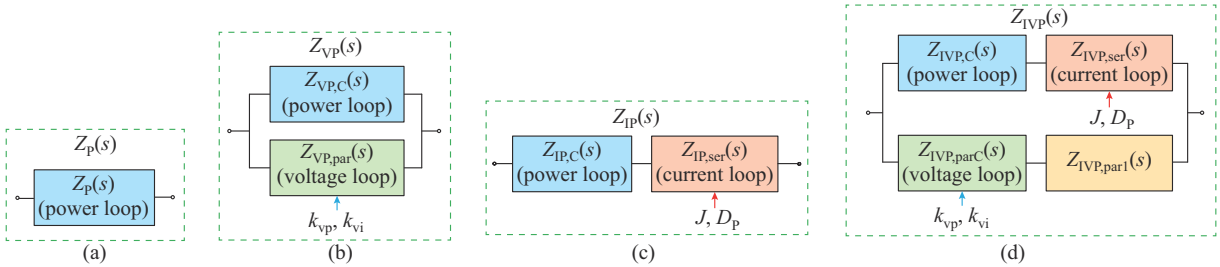

Fig. 9. Schematic diagram of positive-sequence impedances of GFM converters with different control loops. (a) Single power loop. (b) Single voltage loop. (c) Single current loop. (d) Voltage and current dual-loop.

Accordingly, the proposed model aims to streamline the analysis of the impedance characteristics of the multi-loop GFM converter under small-signal stability conditions. By using the proposed model, the characteristics of different inner-loop components can be investigated and enhanced separately, akin to modifying the characteristics of a series or parallel resistance in a circuit to alter the impedance characteristics of the entire circuit. Furthermore, the blue and red arrows in Fig. 9 indicate the parameters that can markedly alter the impedance characteristics of the corresponding control loop. For instance, when the power loop of the GFM converter has been designed, modifications to J and D_p can be made to modify the impedance characteristics of the current loop. Alternatively, the PI parameters of voltage loop can be changed to modify the impedance characteristics of the voltage loop and to indirectly enhance the small-signal stability of the entire multi-loop GFM converter.

Given the impact of interaction between the voltage and current loops on the characteristics of sequence impedance is minimal [27], [28], the element $Z_{IVP,par1}(s)$ can be disregarded. Consequently, through the analysis of the impact between the power loop, voltage loop, and current loop, it is sufficient to modify the small-signal stability of the entire GFM converter.

VI. SIMULATION AND EXPERIMENT

The preceding results are validated through the PLECS simulation and a corresponding prototype experiment.

A. PLECS Simulation

As shown in Fig. 10, in weak grids (with small SCR), GFM converters with single voltage loop demonstrate superior performance compared with those with single current loop. According to the fast Fourier transform (FFT) result, GFM converters with single current loop exhibit low-frequency oscillation at 5-10 Hz when the SCR turns small due to their capacitive impedance characteristics. GFM converters with the single power loop and the voltage and current dual-loop exhibit the results similar to those shown in Fig. 10(a) and (b), respectively. These phenomena further support the conclusion that the GFM converter with a single power loop is the preferred option due to its more straightforward control parameters and superior low-frequency characteristics, particularly in weak grids.

As shown in Fig. 11, when the SCR alters at 4 s and 7 s, the output active power of GFM converter with a single power loop exhibits high-frequency small-signal instability. The harmonic frequency increases as the SCR turns larger, which is consistent with the intersections shown in Fig. 7. GFM converters with alternative control loops manifest anal-

ogous phenomena at high frequencies, thereby substantiating the aforementioned findings.

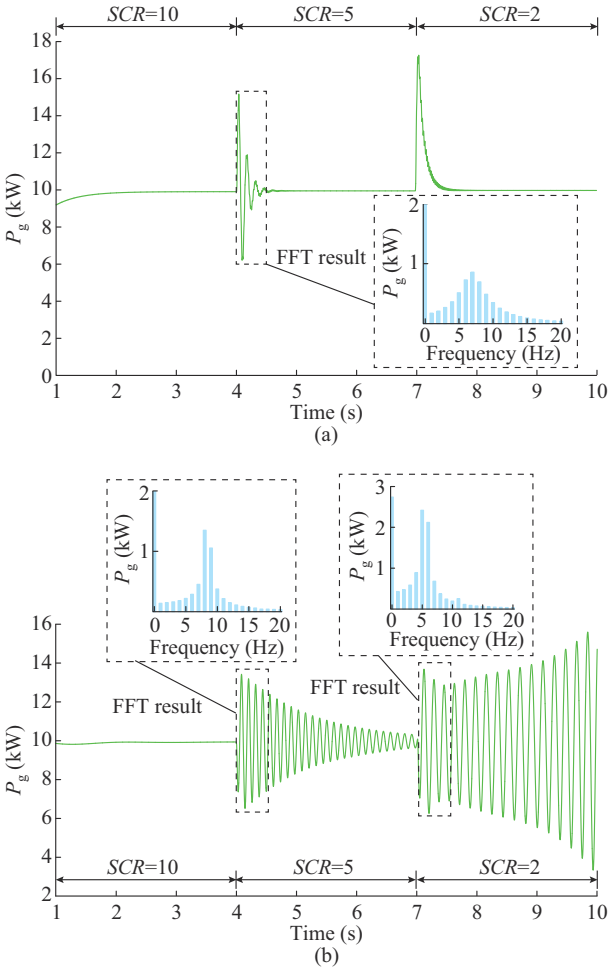

Fig. 10. Low-frequency small-signal instability with different values of SCR. (a) Single voltage loop. (b) Single current loop.

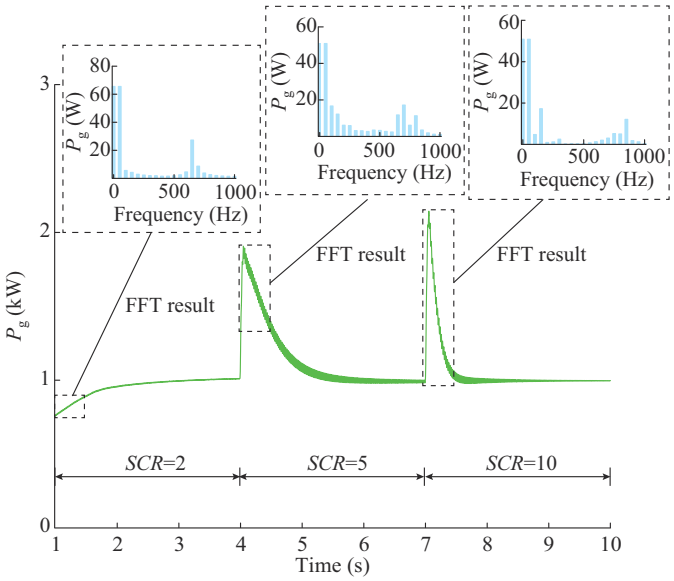

Fig. 11. Output active power of GFM converter with a single power loop with different values of SCR.

B. Prototype Experiment

As shown in Fig. 12, an experimental platform is employed to simulate the actual operational conditions of the GFM converter.

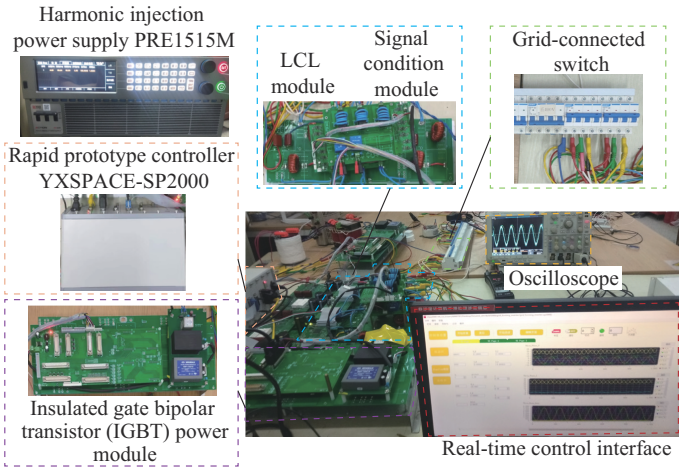

Fig. 12. Experimental platform.

The potential sources of error in the experiments mainly come from: ① sampling error in the measurement of the voltage and current; ② misalignment of the reference frame in the process of measuring the sequence impedance; and ③ a discrepancy between the fundamental frequency of the actual system and the ideal frequency of 50 Hz in the FFT analysis [22].

Nevertheless, under the control of the rapid prototype controller YXSPACE-SP2000 and the corresponding converter device applied in this paper, the synchronized measurements of the three-phase voltages and currents reach a sampling frequency of 20 kHz. Consequently, given that the theoretical and experimental results are in close agreement, it can be concluded that the prototype closely matches the real-world implementation.

A 50 Hz fundamental voltage with an intermittent voltage of varying frequencies is injected by the harmonic injection power supply PRE1515M to conduct a sequence impedance frequency sweep experiment. Subsequently, the FFT is employed to analyze the corresponding voltage and current data, as shown in Fig. 13, to calculate the phase and amplitude and to obtain similar Bode diagrams and characteristics, as shown in Fig. 5.

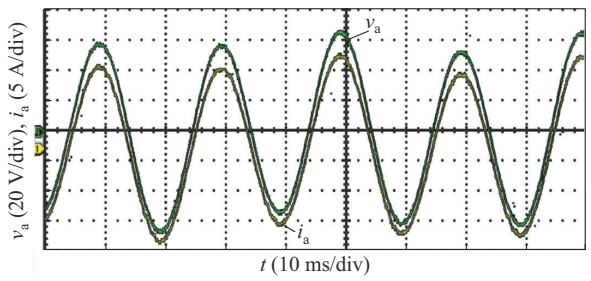

Fig. 13. Voltage and current data for frequency sweep experiment.

As shown in Fig. 14, the low-frequency small-signal insta-

bility of GFM converters occurs with an increase in J from 0.05 to 0.2. This phenomenon is consistent with the aforementioned sensitivity analysis.

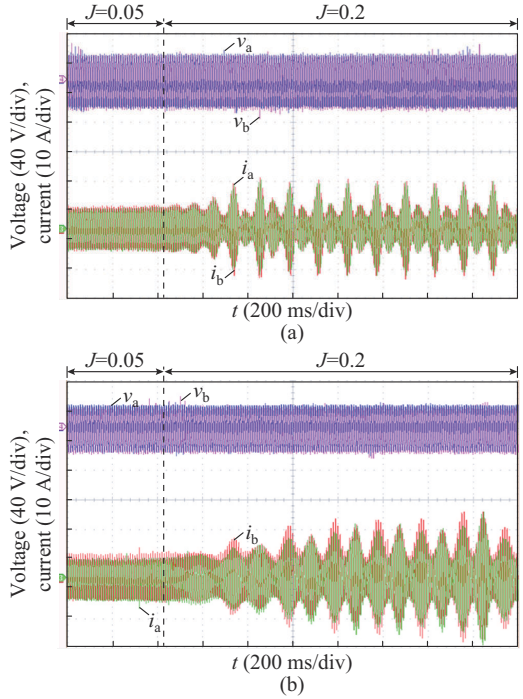

Fig. 14. Low-frequency small-signal instability of GFM converters. (a) Single current loop. (b) Voltage and current dual-loop.

As shown in Fig. 15, the high-frequency small-signal instability of GFM converters occurs when the SCR decreases from 5 to 2. This phenomenon is consistent with the aforementioned high-frequency characteristics in Fig. 7 and Fig. 11.

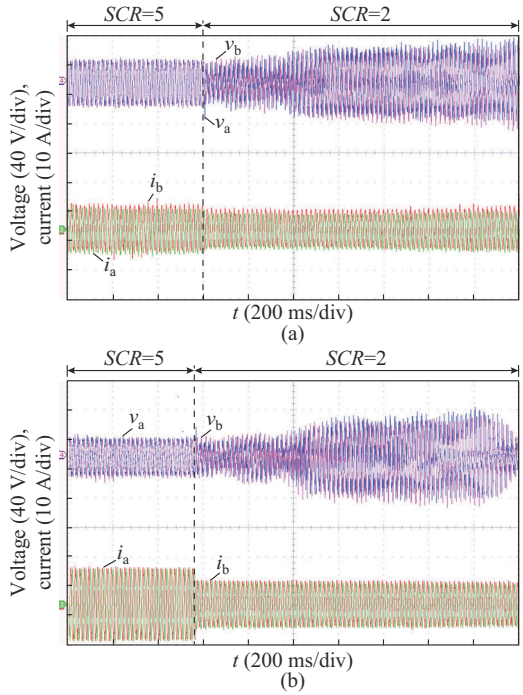

Fig. 15. High-frequency small-signal instability of GFM converters. (a) Single voltage loop. (b) Single current loop.

The preceding experiments further validate that the proposed model of multi-loop GFM converters is an effective means of analyzing their small-signal stability.

VII. Conclusion

This paper presents a series-parallel impedance model of multi-loop GFM converters. The analysis of the small-signal stability of GFM converters through this model allows the derivation of the following results.

1) The sequence impedances of multi-loop GFM converters can be decomposed into impedances in series and in parallel with different control loops. The voltage loop can be conceptualized as impedances in parallel, whereas the current loop can be conceptualized as impedances in series.

2) GFM converters with a single power loop exhibit inductive impedance characteristics at low frequencies. Conversely, the GFM converters with the voltage loop and current loop exhibit capacitive impedance characteristics at low frequencies. Given the relatively small amplitude of the single power loop, the current loop exerts a more considerable influence as parallel impedance than the voltage loop in modifying low-frequency sequence impedances from inductive to capacitive. This may potentially give rise to small-signal instability and low-frequency oscillations, particularly in weak grids.

3) The GFM converters with voltage loop and current loop display capacitive impedance characteristics at high frequencies. The relatively high amplitude of the voltage loop and the relatively low amplitude of the current loop have a negligible impact on the power loop as either parallel or series impedance. Therefore, multi-loop GFM converters display similar high-frequency capacitive impedance characteristics, which may result in high-frequency small-signal instability in both weak and strong grids. Therefore, GFM converters with a single power loop are recommended from the perspective of small-signal stability, since they offer superior low-frequency characteristics in weak grids and simpler parameters.

References

[1] Y. Zhang, B. Liu, C. Lin *et al*., "Equivalent impedance parameter calculation of three-phase symmetrical loads for harmonic source location," *Journal of Modern Power Systems and Clean Energy*, vol. 12, no. 1, pp. 251-260, Jan. 2024.

[2] X. Wang and F. Blaabjerg, "Harmonic stability in power electronic-based power systems: concept, modeling, and analysis," *IEEE Transactions on Smart Grid*, vol. 10, no. 3, pp. 2858-2870, May 2019.

[3] R. Pan, D. Liu, S. Liu *et al*., "Stability comparison between grid-forming and grid-following based wind farms integrated MMC-HVDC," *Journal of Modern Power Systems and Clean Energy*, vol. 11, no. 4, pp. 1341-1355, Jul. 2023.

[4] Y. Li, Y. Gu, and T. C. Green, "Revisiting grid-forming and grid-following inverters: a duality theory," *IEEE Transactions on Power Systems*, vol. 37, no. 6, pp. 4541-4554, Nov. 2022.

[5] M. A. Elshenawy, A. Radwan, and Y. A. R. I. Mohamed, "Unified sequence impedance models of synchronous generator- and virtual oscillator-based grid-forming converters," *IEEE Transactions on Power Delivery*, vol. 39, no. 1, pp. 56-70, Feb. 2024.

[6] Y. Gu, N. Bottrell, and T. C. Green, "Reduced-order models for representing converters in power system studies," *IEEE Transactions on Power Electronics*, vol. 33, no. 4, pp. 3644-3654, Apr. 2018.

[7] M. Farrokhabadi, C. A. Cañizares, J. W. Simpson-Porco *et al*., "Microgrid stability definitions, analysis, and examples," *IEEE Transac-*

tions on Power Systems, vol. 35, no. 1, pp. 13-29, Jan. 2020.
[8] C. Hu, K. Chen, S. Luo *et al*., "Small signal modeling and stability analysis of virtual synchronous generators," in *Proceedings of 2017 20th International Conference on Electrical Machines and Systems*, Sydney, Australia, Aug. 2017, pp. 1-5.
[9] W. Li, J. Wang, J. Song *et al*., "Full-band output impedance model of virtual synchronous generator in *dq* framework," in *Proceedings of 2018 International Power Electronics Conference*, Niigata, Japan, May 2018, pp. 1282-1288.
[10] Y. Li, Y. Gu, Y. Zhu *et al*., "Impedance circuit model of grid-forming inverter: visualizing control algorithms as circuit elements," *IEEE Transactions on Power Electronics*, vol. 36, no. 3, pp. 3377-3395, Mar. 2021.
[11] I. Vieto and J. Sun, "Sequence impedance modeling and converter-grid resonance analysis considering DC bus dynamics and mirrored harmonics," in *Proceedings of 2018 IEEE 19th Workshop on Control and Modeling for Power Electronics*, Padua, Italy, Jun. 2018, pp. 1-8.
[12] A. Rygg, M. Molinas, C. Zhang *et al*., "A modified sequence-domain impedance definition and its equivalence to the *dq*-domain impedance definition for the stability analysis of AC power electronic systems," *IEEE Journal of Emerging and Selected Topics in Power Electronics*, vol. 4, no. 4, pp. 1383-1396, Dec. 2016.
[13] J. Sun, G. Wang, X. Du *et al*., "A theory for harmonics created by resonance in converter-grid systems," *IEEE Transactions on Power Electronics*, vol. 34, no. 4, pp. 3025-3029, Apr. 2019.
[14] M. Cespedes and J. Sun, "Impedance modeling and analysis of grid-connected voltage-source converters," *IEEE Transactions on Power Electronics*, vol. 29, no. 3, pp. 1254-1261, Mar. 2014.
[15] W. Wu, Y. Chen, L. Zhou *et al*., "Sequence impedance modeling and stability comparative analysis of voltage-controlled VSGs and current-controlled VSGs," *IEEE Transactions on Industrial Electronics*, vol. 66, no. 8, pp. 6460-6472, Aug. 2019.
[16] Y. Peng, T. Yin, M. Li *et al*., "A sequence impedance modeling of VSG with consideration of inner loops control," in *Proceedings of 2019 4th IEEE Workshop on the Electronic Grid*, Xiamen, China, Nov. 2019, pp. 1-5.
[17] M. Dokus and A. Mertens, "Sequence impedance characteristics of grid-forming converter controls," in *Proceedings of 2020 IEEE 11th International Symposium on Power Electronics for Distributed Generation Systems*, Dubrovnik, Croatia, Sept. 2020, pp. 413-420.
[18] K. Shi, Y. Wang, Y. Sun *et al*., "Frequency-coupled impedance modeling of virtual synchronous generators," *IEEE Transactions on Power Systems*, vol. 36, no. 4, pp. 3692-3700, Jul. 2021.
[19] H. Wang, Z. Xie, Y. Chen *et al*., "Admittance-based stability analysis of current-controlled VSG considering the frequency coupling characteristics," *IEEE Journal of Emerging and Selected Topics in Power Electronics*, vol. 11, no. 1, pp. 1191-1202, Feb. 2023.
[20] Y. Liu, Y. Wang, Y. Peng *et al*., "Unified modeling and analysis of sequence impedance of grid-forming converters with multi-loop control," in *Proceedings of 2021 IEEE/IAS Industrial and Commercial Power System Asia*, Chengdu, China, Jul. 2021, pp. 118-124.
[21] N. Liu, H. Wang, L. Sun *et al*., "Modular impedance modeling and stability analysis of hybrid AC/DC power systems with grid-forming and grid-following converters," *IEEE Access*, vol. 12, pp. 4063-4077, Jan. 2024.
[22] S. Shah, P. Koralewicz, V. Gevorgian *et al*., "Sequence impedance measurement of utility-scale wind turbines and inverters – reference frame, frequency coupling, and MIMO/SISO forms," *IEEE Transactions on Energy Conversion*, vol. 37, no. 1, pp. 75-86, Mar. 2022.
[23] Z. Guo, X. Zhang, M. Li *et al*., "Stability analysis and capacity distribution of multi-paralleled current-controlled inverters and voltage-controlled VSGs grid-connected system," in *Proceedings of 2021 IEEE 12th International Symposium on Power Electronics for Distributed Generation Systems*, Chicago, USA, Jun. 2021, pp. 1-8.
[24] B. Kong, J. Zhu, S. Wang *et al*., "Comparative study of the transmission capacity of grid-forming converters and grid-following converters," *Energies*, vol. 16, no. 6, p. 2594, Mar. 2023.
[25] Z. Zou, J. Tang, X. Wang *et al*., "Modeling and control of a two-bus system with grid-forming and grid-following converters," *IEEE Journal of Emerging and Selected Topics in Power Electronics*, vol. 10, no. 6, pp. 7133-7149, Dec. 2022.
[26] Y. Yang, Z. Zhou, L. Zhao *et al*., "Controller sensitivity-based shaping method for grid forming inverter," in *Proceedings of 2023 IEEE Energy Conversion Congress and Exposition*, Nashville, USA, Oct. 2023, pp. 6273-6278.
[27] M. Huang, C. K. Tse, S. C. Wong *et al*., "Low-frequency Hopf bifurcation and its effects on stability margin in three-phase PFC power supplies connected to non-ideal power grid," *IEEE Transactions on Circuits and Systems I*: *Regular Papers*, vol. 60, no. 12, pp. 3328-3340, Dec. 2013.
[28] Y. Liu, M. Huang, L. Qu *et al*., "Interaction of voltage and current control loop in three-phase voltage source converter," in *Proceedings of 43rd Annual Conference of the IEEE Industrial Electronics Society*, Beijing, China, Oct. 2017, pp. 6847-6852.

Xiaokuan Jin received the B.S. degree in electrical engineering from Nanjing Institute of Technology, Nanjing, China, in 2022. Since 2022, he is pursuing the M.S. degree at the School of Electrical Engineering, Southeast University, Nanjing, China, majoring in power electronics technology. His main research interests include impedance modeling and stability analysis of power grid, and efficiency optimization analysis of compressed air energy storage systems.

Jianhua Wang received the B.S. and Ph.D. degrees in electrical engineering from Nanjing University of Aeronautics & Astronautics, Nanjing, China, in 2004 and 2010, respectively. In 2010, he joined the School of Electrical Engineering in Southeast University, Nanjing, China, where he is currently an Associate Professor. His main research interests include solid-state transformer, power electronic system stability, distributed generation, and microgrid.

Han Yan received the B.S. degree from Southeast University, Nanjing, China, in 2016, and the M.S. degree from Nanjing University of Science and Technology, Nanjing, China, in 2020. He is currently pursuing the Ph.D. degree in electrical engineering, Southeast University. His main research interests include hybrid transformer, power electronic system stability, and distribution system restoration.

Xijun Ni received the Ph.D. degree in electrical engineering from Southeast University, Nanjing, China, in 2011. From 2011 to 2015, he was a Postdoctoral Research Scholar in the Future Renewable Electric Energy Delivery and Management Systems Center, Department of Electrical and Computer Engineering, North Carolina State University, Raleigh, USA. He is currently an Assistant Professor with the Nanjing Institute of Technology, Nanjing, China. His research interests include modulation and control of multilevel converter, wide band gap device and its applications, and modern digital control technique.

Zhendong Ji received the B.S. and Ph.D. degrees in electrical engineering from Southeast University, Nanjing, China, in 2007 and 2015, respectively. Since 2015, he joined the School of Automation, Nanjing University of Science and Technology, Nanjing, China, where he is currently an Associate Professor. His main research interests include cascade multilevel converter and solid-state transformer.

Baojian Ji received the B. S. degree in automation engineering from the Nanjing Normal University, Nanjing, China, in 2002, the M. S. degree in electrical engineering from the Nanjing University of Aeronautics and Astronautics, Nanjing, China, in 2007, and the Ph.D. degree from Southeast University, Nanjing, China, in 2012. In 2016, he became an Associate Professor at Nanjing University of Science and Technology, Nanjing, China. His current research interests include high-power-density power supply and high-voltage power supply.

Ding Wan received the B.S. degree in electrical engineering from Nanjing Forestry University, Nanjing, China, in 2023. He is currently pursuing the M. S. degree in electrical engineering at Nanjing Institute of Technology, Nanjing, China. His research interests include stability analysis and virtual inertia optimization of grid-connected inverters, power quality optimization based on inverters, and intelligent control of inverters.